(Received 5 March 2026, Accepted 7 April 2026, Scheduled 26 April 2026)

Design and Analysis of High-Selectivity Microstrip Bandpass Filters with Controllable Transmission Zeros

Chuan Shao[1,*], Xin Gao[2], Rong Cai[1], Ke Wang[1], Xinnai Zhang[1], and Kai Xu[3]

[1]*Nantong Key Laboratory of Artificial Intelligence New Quality Technology Jiangsu College of Engineering and Technology, Nantong 226000, Jiangsu, China*
[2]*Shanghai Institute of Satellite Engineering, Shanghai 201109, China*
[3]*Nantong Key Laboratory of Advanced Microwave Technology, Nantong University, Nantong 226019, Jiangsu, China*

ABSTRACT: In this paper, a series of high-selectivity bandpass filters based on parallel-coupled microstrip lines is proposed. The developed filters are derived from a conventional parallel-coupled microstrip line filter, with an additional pair of parallel-coupled microstrip lines incorporated into the two open ends, one of which is short-circuited. Accordingly, a pair of transmission zeros is introduced into the transmission coefficient of the traditional parallel-coupled microstrip line filter by this modification, thereby enhancing its selectivity. To further enhance the selectivity of the developed filter, a pair of quarter-wavelength transmission lines was connected to each of the short-circuited ends. This additional structure introduces another pair of transmission zeros, thereby further improving the selectivity of the filter. For demonstration, two bandpass filters have been designed and fabricated. Specifically, the measured attenuation slopes for the modified structure were 213 dB/GHz and 106 dB/GHz at the lower and upper band edges, respectively.

1. INTRODUCTION

In modern microwave communication systems, microwave filters are essential passive components that have garnered significant interest from microwave and radio frequency (RF) researchers. For microwave bandpass filters, high selectivity is a crucial performance metric, along with other important parameters, such as low insertion loss, high out-of-band rejection, and compact size [1, 2].

To enhance the selectivity of a bandpass filter, three approaches are generally used. The first approach involves increasing the order of the bandpass filter. However, increasing the order of the filter typically results in an enlarged circuit size. Consequently, this method is generally not preferred because of its disadvantages [3–6]. The second method involves the use of high-Q transmission line structures. However, high-Q transmission lines, such as waveguide structures, are often bulky and difficult to manufacture [7, 8].

The final technique for boosting selectivity involves increasing the number of transmission zeros for the bandpass filter, which effectively narrows the passband and sharply attenuates the stopband frequencies. Generally, two primary methods can be employed to introduce additional transmission zeros in the transfer function. The first approach is to increase the number of signal transmission paths, such as by employing cross-coupling [9–13]. The second approach involves generating additional transmission zeros through the use of parallel resonators, such as spurlines [14] or defected ground structures [15, 16]. For cross-coupled filters in [9–13], the requirement to satisfy specific coupling structures often results in relatively large dimensions, as the number of transmission zeros (M) is generally limited to $N-2$, where N denotes the filter order. Moreover, the corresponding coupling matrix is required to be obtained. For bandpass filters employing open-circuited stubs or spurlines at the ports [14], the overall size is typically large. For bandpass filters utilizing defected ground structures [15, 16], the integrity of the ground plane is compromised. Consequently, designing high-selectivity bandpass filters with simple structures and compact sizes remains a significant challenge owing to the inherent trade-offs and complexities associated with each approach.

In this paper, a series of high-selectivity bandpass filters is developed using parallel-coupled microstrip lines. Closed-form expressions for the resonant frequencies are derived to guide practical implementation. Moreover, the newly generated pair of transmission zeros can be adjusted by varying the characteristic impedance of the quarter-wavelength transmission lines, which can be utilized to suppress signals at specific frequencies outside the passband.

2. DESIGN OF ANALYSIS FOR THE PROPOSED FILTERS

The structure of the conventional parallel-coupled microstrip line bandpass filter is illustrated in Fig. 1, and its simulated performance is depicted in Fig. 2. As can be observed, the filter exhibits relatively poor frequency selectivity. Furthermore, the out-of-band rejection performance was found to be inadequate,

* Corresponding author: Chuan Shao (ch_shao@126.com).

FIGURE 1. Conventional bandpass filter using parallel-coupled microstrip lines.

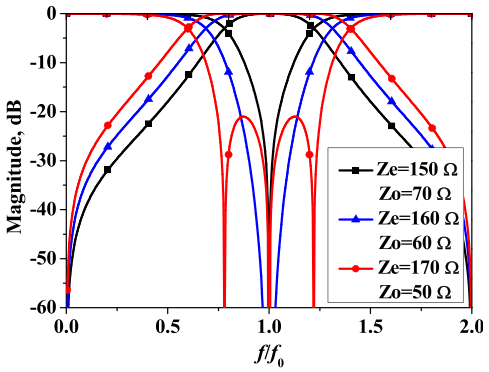

FIGURE 2. Simulated responses of the structure in Fig. 1.

thereby limiting its suitability for applications requiring high spectral purity.

To enhance the selectivity and out-of-band rejection performance, a pair of quarter-wave-length-coupled microstrip lines, one end of which is short-circuited, is inserted between the two open-circuited ends of the conventional parallel-coupled microstrip line bandpass filter, as illustrated in Fig. 3. For convenience analysis, the odd- and even-mode impedances of the two sets of parallel coupled microstrip lines are set to be identical.

Because the developed bandpass filter has a symmetrical structure, it can be decomposed into even- and odd-mode excitations, shown in Fig. 4. For the even-mode equivalent circuit, its input admittance can be obtained as follows:

$$Z_{\text{ine}} = \frac{A_e \cdot Z_{\text{in1}} + B_e}{C_e \cdot Z_{\text{in1}} + D_e} \tag{1}$$

where A_e, B_e, C_e, D_e are the transfer matrix elements of the two-port network enclosed by the dashed box in Fig. 4(b), and Z_{in1} is the input impedance of a transmission line with characteristic impedance Z_e, electrical length θ, and one end short-circuited. As discussed in [17], the transfer matrix of the two-port network can be derived as follows:

$$\begin{pmatrix} A_e & B_e \\ C_e & D_e \end{pmatrix} = \begin{pmatrix} \cos\theta & j\frac{Z_e+Z_o}{2}\sin\theta \\ j\frac{2\sin\theta}{Z_e+Z_o} & \cos\theta \end{pmatrix} \tag{2}$$

Therefore, the input admittance for the even-mode equivalent is expressed as

$$Z_{\text{ine}} = j\frac{(3Z_e+Z_o)(Z_e+Z_o)\sin\theta\cos\theta}{2\left[(Z_e+Z_o)\cos^2\theta - 2Z_e\sin^2\theta\right]} \tag{3}$$

Similarly, the input admittance for the even-mode equivalent can be represented as

$$Z_{\text{ino}} = \frac{A_o \cdot Z_{\text{in2}} + B_o}{C_o \cdot Z_{\text{in2}} + D_o} = j\sin\theta$$

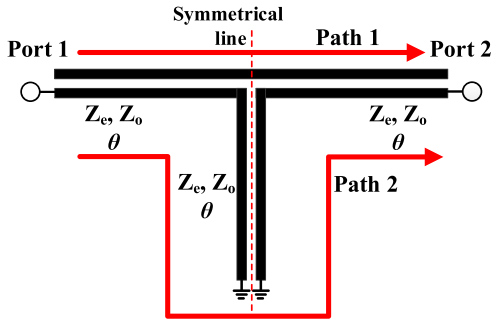

FIGURE 3. Schematic of the developed bandpass filter based on the structure in Fig. 1.

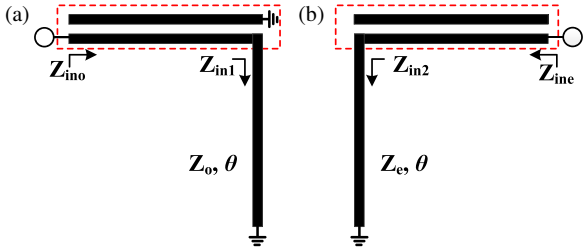

FIGURE 4. Equivalent circuits for the developed bandpass filter, (a) odd mode, (b) even mode.

$$\cdot \left(\frac{\frac{(Z_e+Z_o)^2\cos^2\theta-(Z_e-Z_o)^2}{4Z_e} + \frac{Z_e+Z_o}{2}\cos\theta}{\cos^2\theta - \frac{Z_e+Z_o}{2Z_e}\sin^2\theta} \right) \tag{4}$$

where A_o, B_o, C_o, D_o are the transfer matrix elements of the two-port network enclosed by the dashed box in Fig. 4(a), and Z_{in2} is the input impedance of a transmission line with characteristic impedance Z_o, electrical length θ, and one end short-circuited.

$$\begin{pmatrix} A_o & B_o \\ C_o & D_o \end{pmatrix} = \begin{pmatrix} \frac{(Z_e+Z_o)^2\cos^2\theta-(Z_e-Z_o)^2}{4Z_eZ_o\cos\theta} & j\frac{Z_e+Z_o}{2}\sin\theta \\ j\frac{Z_e+Z_o}{2Z_eZ_o}\sin\theta & \cos\theta \end{pmatrix} \tag{5}$$

When $Y_{\text{ine}} = 1/Z_{\text{ine}}$, $Y_{\text{ino}} = 1/Z_{\text{ino}}$ equals zero, and five roots can be obtained, which are derived as

$$\theta_1 = \arctan\sqrt{\frac{Z_e+Z_o}{2Z_e}} \tag{6}$$

$$\theta_2 = \arctan\sqrt{\frac{2Z_e}{Z_e+Z_o}} \tag{7}$$

$$\theta_3 = \frac{\pi}{2} \tag{8}$$

$$\theta_4 = \pi - \theta_2 \tag{9}$$

$$\theta_5 = \pi - \theta_1 \tag{10}$$

In addition, when $Z_{\text{ine}} = Z_{\text{ino}}$, two transmission zeros located at DC and $2f_0$ can be straightforwardly identified from the circuit symmetry and boundary conditions. Unfortunately, due to the high-order nature of the governing equations — a quartic (fourth-order) polynomial equation in the frequency variable —

it is mathematically intractable to obtain closed-form analytical solutions for the remaining two finite-frequency transmission zeros. However, the remaining two finite-frequency transmission zeros cannot be expressed in explicit analytical form in terms of Z_e and Z_o.

To illustrate the impact of the odd-mode and even-mode impedances on the filter, Fig. 5 shows the S-parameters for various combinations of odd-mode and even-mode impedances. As shown in Fig. 5, with a gradual increase in the coupling coefficient $C = (Z_e+Z_o)/(Z_e-Z_o)$, the operating bandwidth of the developed bandpass filter gradually increases, whereas the out-of-band rejection performance deteriorates progressively. Specifically, these transmission zeros originate from the signal cancellation (interference) technique, which may also be characterized as multi-path interference as shown in Fig. 3 [18, 19].

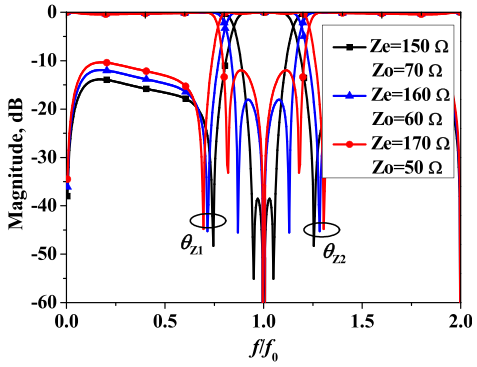

FIGURE 5. Responses for the original structure of the developed bandpass filter.

Moreover, considering the limitations of the manufacturing processes, the selected odd-mode and even-mode impedances are respectively as $Z_e = 150\,\Omega$, $Z_o = 70\,\Omega$. Notably, the transmission poles θ_1 and θ_5, which are supposed to generate resonant points outside the passband and thereby degrade the out-of-band rejection characteristics, are effectively suppressed owing to the presence of transmission zeros on both sides of the passband.

To further enhance the selectivity of the developed bandpass filter under the same coupling coefficient conditions, a pair of quarter-wavelength transmission lines with characteristic impedance of Z_s is connected to each of the short-circuited ends, as depicted in Fig. 6. Similarly, the modified structure of the developed bandpass filter was also axially symmetric. Therefore, by performing an odd-even mode analysis, the corresponding equivalent circuits can be obtained, as shown in Fig. 7.

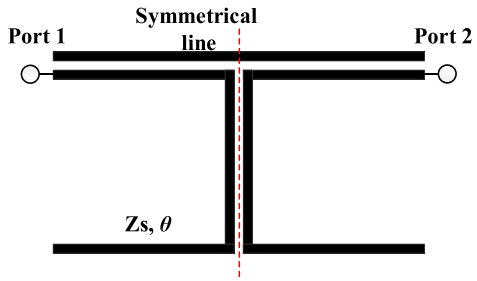

FIGURE 6. Schematic of the modified structure for the developed bandpass filter.

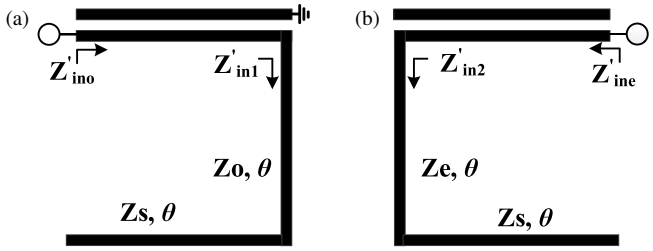

FIGURE 7. Equivalent circuits for the modified structure for the developed bandpass filter, (a) odd mode, (b) even mode.

Referring to the aforementioned analysis, the even-mode and odd-mode input impedances Z'_{ine} and Z'_{ino} in Fig. 7 are

$$Z'_{\text{ine}} = \frac{A_e \cdot Z'_{\text{in1}} + B_e}{C_e \cdot Z'_{\text{in1}} + D_e} \tag{11}$$

$$Z'_{\text{ino}} = \frac{A_o \cdot Z'_{\text{in2}} + B_o}{C_o \cdot Z'_{\text{in2}} + D_o} \tag{12}$$

where Z'_{in1} and Z'_{in2} can be derived as

$$Z'_{\text{in1}} = Z_e \frac{Z_e \tan^2\theta - Z_s}{(Z_e + Z_s)\tan\theta} \tag{13}$$

$$Z'_{\text{in2}} = Z_o \frac{Z_o \tan^2\theta - Z_s}{(Z_o + Z_s)\tan\theta} \tag{14}$$

Given the high order of the aforementioned equations, explicit solutions cannot be obtained readily. Consequently, a parametric sweep analysis was employed to investigate the behavior.

The responses of the original and modified structures of the developed bandpass filters are illustrated in Fig. 8. It can be observed that, after the incorporation of open-circuit stubs, two additional transmission zeros are generated. These zeros effectively enhance the out-of-band rejection level and improve the selectivity within the passband of the bandpass filter.

To investigate the influence of Z_e, Z_o, and Z_s on the modified structure, the control variable method is employed. When Z_e and Z_o are maintained constant, the filter response versus

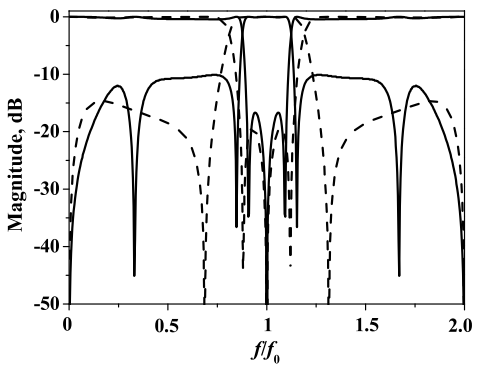

FIGURE 8. Responses for the modified and original structures of the developed bandpass filters. ($Z_e = 150\,\Omega$, $Z_o = 70\,\Omega$, $Z_s = 100\,\Omega$).

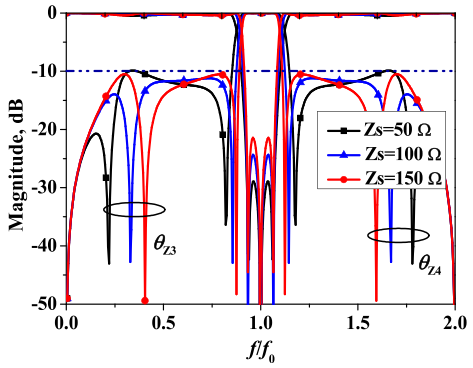

FIGURE 9. Responses for the modified structure of the developed bandpass filter versus Z_s. ($Z_e = 150\,\Omega$, $Z_o = 70\,\Omega$).

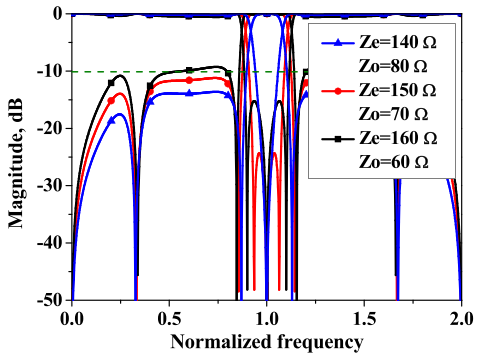

FIGURE 10. Responses for the modified structure of the developed bandpass filter versus Z_e and Z_o. ($Z_s = 130\,\Omega$).

Z_s is presented in Fig. 9. As can be seen from the figure, with the gradual increase in Z_s, all the transmission zeros except those at DC and $2f_0$ are observed to move towards the center frequency, thereby further enhancing the selectivity within the passband. However, regarding the transmission zeros θ_{Z1} and θ_{Z2}, their variation ranges are considerably smaller than those of θ_{Z3} and θ_{Z4} when Z_s is adjusted. Consequently, it can be concluded that the transmission zeros θ_{Z1} and θ_{Z2} remain essentially unchanged during the tuning of Z_s. According to [20], the maximum available characteristic impedance of microstrip lines is limited to approximately $130\,\Omega$. Considering the constraints of manufacturing processes, Z_s is selected to be $130\,\Omega$.

When the characteristic impedance of the open-circuited stub Z_s is fixed, the four transmission zeros excluding the two located at DC and $2f_0$ can be tuned by adjusting Z_e and Z_o, as demonstrated in Fig. 10. According to Fig. 10, it is evident that when the coupling coefficient C is varied, the transmission zeros θ_{Z3} and θ_{Z4} can be regarded as essentially unchanged compared to the variation ranges of θ_{Z1} and θ_{Z2}. Therefore, it can be concluded that the transmission zeros θ_{Z3} and θ_{Z4} remain substantially unaffected when the coupling coefficient C is adjusted.

To sum up, the proposed structure adopts a distinct loading approach by introducing parallel-coupled microstrip lines with one short-circuited end at the open ends of the coupled resonators, thereby establishing dual signal propagation paths to generate additional transmission zeros. While this achieves the same goal of enhancing filter selectivity as conventional port-loaded stubs, the implementation methodology is fundamentally different from both center-loaded and port-loaded configurations [21–24].

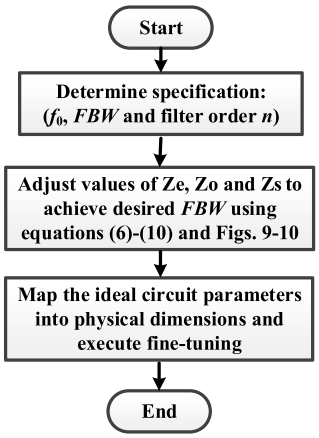

FIGURE 11. Flowchart for the developed bandpass filter.

To guide the practical filter implementation in Fig. 10 and based on the flowchart given in Fig. 11, the following procedure can be obtained:

1. Determine the fractional bandwidth (FBW), center frequency (f_0), and filter order (n) of the proposed filter.
2. Based on Equations (5)–(10) and Figs. 9–10, adjust the even-mode impedance (Z_e), odd-mode impedance (Z_o), and source impedance (Z_s) to satisfy the aforementioned specifications.
3. Employ the Linecalc tool in Keysight advanced design system (ADS) to calculate the corresponding physical dimensions based on the selected substrate parameters, followed by fine-tuning to optimize performance.

3. RESULTS AND DISCUSSION

In this design, the center frequency is determined to be 3 GHz, and the substrate employed was Rogers 4003c (loss tangent of 0.0027, dielectric constant of 3.55, and thickness of 0.508 mm). Consequently, based on the preceding analysis and design, the modified structure of the developed bandpass filter has been laid out and fabricated as depicted in Fig. 12.

The simulated and measured S-parameters for the original structure of the developed bandpass filter are plotted in Fig. 13. The operating passband width of the developed bandpass filter is 0.75 GHz, which corresponds to 25% in fraction. Owing to the fabrication errors, the out-of-band rejection at the high-frequency end of the filter exhibited slight deviations from the simulated results, thereby affecting the selectivity of the filter to a certain extent.

A comparison between the simulated and tested results for the modified structure of the developed bandpass filter is illustrated in Fig. 14. Similar to the original structure, the out-of-band rejection at the high-frequency end of this filter also exhibited some discrepancies from the simulated results. However, these differences have almost no impact on the passband selectivity of the filter. As shown in this figure, the operating bandwidth of the filter is approximately 600 MHz, corresponding to

TABLE 1. Comparison with previously reported structures.

Ref.	f_0	Insertion Loss, dB	Filter Order	Transmission zeros	CZ*	AS** dB/GHz	Technology	Size $\lambda_g \times \lambda_g$
[4]	5.4	1.2	4	4	NO	90/80	MSL	0.5×0.35
[5]	7.35	0.5	14	4	NO	104/518	HTS	0.45×0.4
[6]	2.5	0.8	7	4	NO	160/200	MSL	1×0.165
[7]	3	2	5	6	NO	99/89	RDW	0.87×0.63
[13]	28	2	3	4	YES	114/105	SIW	0.98×0.97
[14]	3.74	0.76	5	4	NO	74/65	MSL	1.6×0.55
This work	3	0.7	3	6	YES	213/106	MSL	0.5×0.25

* CZ is short for Controllable zeros.
** AS is short for Attenuation slope.

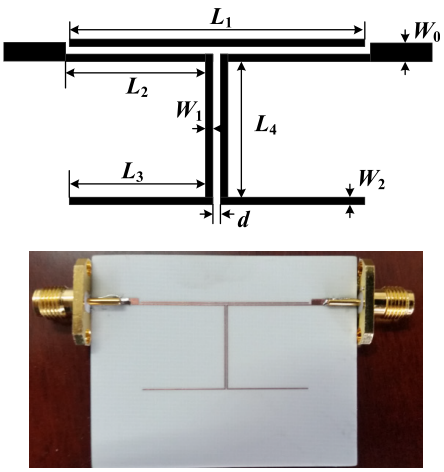

FIGURE 12. Layout and photograph of the modified structure of the developed bandpass filter. ($L_1 = 32$ mm, $L_2 = 16$ mm, $L_3 = 16$ mm, $L_4 = 16$ mm, $W_0 = 1.1$ mm, $W_1 = 0.2$ mm, $W_2 = 0.1$ mm, $d = 0.2$ mm).

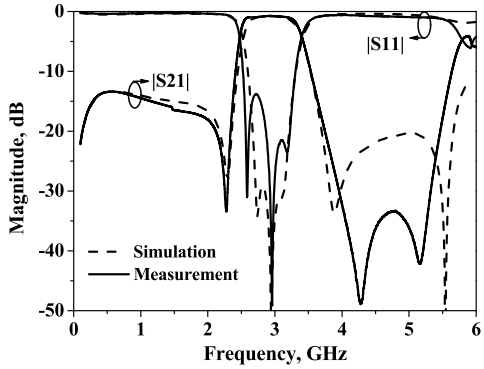

FIGURE 13. Simulated and measured results of the original structure of the developed high-selectivity bandpass filter.

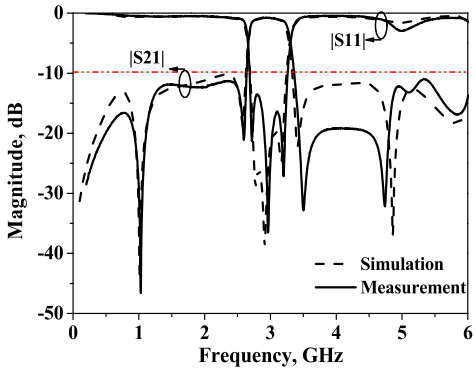

FIGURE 14. Simulated and measured results of the modified structure of the developed high-selectivity bandpass filter.

a relative bandwidth of 20%. The measured lower band edge attenuation slope was 213 dB/GHz, and the upper band edge attenuation slope was 106 dB/GHz, which indicates that the designed filter possesses superior passband selectivity. In addition, two additional transmission zeros are generated at 1 GHz and 4.8 GHz, respectively, with suppression depths exceeding 30 dB. The consistency between the full-wave simulation and theoretical predictions validates the practical feasibility of the proposed structure, confirming that the observed discrepancies are attributable to the inherent differences between ideal circuit models and electromagnetic reality.

Although better out-of-band suppression could be achieved by cascading multi-stage filters, the original design objective was to realize high selectivity with controllable transmission zeros using the minimum number of stages, and the attenuation level exceeding 10 dB across the entire operating frequency band is still regarded as acceptable for many practical applications.

In order to clearly demonstrate the performance advantages of the bandpass filter proposed in this study, Table 1 provides a comparison of the key metrics of the proposed microstrip line (MSL) bandpass filters with those of previously reported state-of-the-art counterparts characterized by different orders and various transmission line types, including ridged dielectric waveguide (RDW), substrate integrated waveguide (SIW), and high-temperature superconducting (HTS) microstrip lines.

As shown in Table 1, compared with previously reported high-selectivity bandpass filters realized on diverse transmission lines, the developed filter, implemented in a single-layer substrate, achieves superior passband selectivity and flexible transmission zero control with the same or even fewer resonator stages than conventional higher-order designs, while demonstrating that satisfactory selectivity and independently tunable transmission zeros can be realized without relying on high-Q resonators or complex cross-coupling schemes.

4. CONCLUSION

In this study, a series of high-selectivity bandpass filters based on parallel-coupled microstrip lines was proposed. By incorporating additional parallel-coupled microstrip lines and quarter-wavelength transmission lines, the developed filters achieved enhanced selectivity by introducing multiple transmission zeros. In particular, the attenuation slopes are measured to be 213 dB/GHz at the lower band edge and 106 dB/GHz at the upper band edge, respectively. Closed-form expressions for the resonant frequencies have been derived, enabling practical implementation and frequency adjustment.

ACKNOWLEDGEMENT

This work was supported by the National Natural Science Foundation of China under Grant 62201291, the Educational Research Project of the Nantong Vocational and Technical Education Association (Grants NTZJXH2504 and NTZJXH2528), the Natural Science and Technology Project of Jiangsu College of Engineering and Technology (Grant JSGYZRJJZD-03) and the Nantong Natural Science Foundation Project (Grants JCZ2025029 and JC2025042).

REFERENCES

[1] Aidoo, M. W., K. Song, and Y. Fan, "High selectivity wideband two-channel bandpass filter for 5G microwave communication systems," *Microwave and Optical Technology Letters*, Vol. 66, No. 10, e34289, 2024.

[2] Yan, J.-M., A.-Q. Tong, and L.-Z. Cao, "Design of a compact microstrip box-like bandpass filter with high-frequency selectivity and excellent stop-band performance," *Microwave and Optical Technology Letters*, Vol. 67, No. 8, e70340, 2025.

[3] Pozar, D. M., *Microwave Engineering*, 4th ed., John Wiley & Sons, Hoboken, NJ, USA, 2012.

[4] Ramkumar, S. and R. B. Rani, "Compact high-selective wide-stopband coupled bandpass filter using middle-shorted hairpin-resonators," *AEU — International Journal of Electronics and Communications*, Vol. 162, 154580, 2023.

[5] Lu, X., X. Fang, G. Wei, S. Zhou, L. Sun, X. Bai, B. Weng, Y. Gao, and D. Chen, "High selectivity wideband superconducting filter design based on feed line resonator (FLR) method," *IEEE Microwave and Wireless Technology Letters*, Vol. 34, No. 9, 1079–1082, Sep. 2024.

[6] Kanaparthi, V. P. K., V. K. Velidi, R. Rajkumar, *et al.*, "A compact ultra-wideband multimode bandpass filter with sharp-rejection using stepped impedance open stub and series transformers," *IEEE Transactions on Circuits and Systems II: Express Briefs*, Vol. 69, No. 12, 4824–4828, Dec. 2022.

[7] Lu, L.-X., Y.-K. Zhou, W. Qin, W.-W. Yang, and J.-X. Chen, "A novel and compact dual-orthogonal-ridged dielectric waveguide resonator and its applications to bandpass filters," *IEEE Transactions on Microwave Theory and Techniques*, Vol. 73, No. 3, 1671–1679, Mar. 2025.

[8] Tang, W. S., Y.-M. Zhang, S. Y. Zheng, and Y. M. Pan, "Low-cost compact inline single-/dual-band filters based on dual-mode dielectric resonators with highly integrated and flexible mixed couplings," *IEEE Transactions on Microwave Theory and Techniques*, Vol. 73, No. 9, 6589–6602, Sep. 2025.

[9] Shaman, H. and J.-S. Hong, "Input and output cross-coupled wideband bandpass filter," *IEEE Transactions on Microwave Theory and Techniques*, Vol. 55, No. 12, 2562–2568, Dec. 2007.

[10] Choi, H., M. Song, and J. Lee, "Novel transmission-line circuit configuration of cross-coupled filter with negative coupling," *IEEE Transactions on Microwave Theory and Techniques*, Vol. 72, No. 8, 4842–4853, Aug. 2024.

[11] Chu, P., J. Zhou, W. Zhang, F. Zhu, L. Cheng, L. Liu, and K. Wu, "Cross coupled substrate integrated waveguide filter with quasi elliptic response and wide stopband," *IEEE Transactions on Components, Packaging and Manufacturing Technology*, Vol. 15, No. 8, 1726–1731, Aug. 2025.

[12] Hong, J.-S. and M. J. Lancaster, "Cross-coupled microstrip hairpin-resonator filters," *IEEE Transactions on Microwave Theory and Techniques*, Vol. 46, No. 1, 118–122, Jan. 1998.

[13] Liu, H., L. Chen, S. Wu, M. Mao, H. Baxter, B. Yang, W. Li, and K. Song, "A new electric coupling and its applications on millimeter-wave SIW filter with high selectivity and controllable TZs," *AEU — International Journal of Electronics and Communications*, Vol. 173, 154989, 2024.

[14] Zhang, X., Y. Wu, H. Yu, W. Wang, Y. Yang, and J. Gao, "High selectivity wideband bandpass filters based on flexibly transferring the structure of a coupled-line," *AEU — International Journal of Electronics and Communications*, Vol. 155, 154334, 2022.

[15] Lin, W.-J., J.-Y. Li, L.-S. Chen, D.-B. Lin, and M.-P. Houng, "Investigation in open circuited metal lines embedded in defected ground structure and its applications to UWB filters," *IEEE Microwave and Wireless Components Letters*, Vol. 20, No. 3, 148–150, Mar. 2010.

[16] Luo, X., J.-G. Ma, and E.-P. Li, "Hybrid microstrip/DGS cell for filter design," *IEEE Microwave and Wireless Components Letters*, Vol. 21, No. 10, 528–530, Oct. 2011.

[17] Matthaei, G. L., L. Young, and E. M. T. Jones, *Microwave Filters, Impedance-matching Networks, and Coupling Structures*, Artech House, Mountain View, CA, USA, 1980.

[18] Gomez-Garcia, R., M. Sanchez-Renedo, B. Jarry, J. Lintignat, and B. Barelaud, "A class of microwave transversal signal-interference dual-passband planar filters," *IEEE Microwave and Wireless Components Letters*, Vol. 19, No. 3, 158–160, Mar. 2009.

[19] Gomez-Garcia, R. and J. I. Alonso, "Design of sharp-rejection and low-loss wide-band planar filters using signal-interference techniques," *IEEE Microwave and Wireless Components Letters*, Vol. 15, No. 8, 530–532, Aug. 2005.

[20] Bahl, I. J. and D. K. Trivedi, "A designer's guide to microstrip line," *Microwaves*, Vol. 16, No. 5, 174–182, May 1977.

[21] Li, R. and L. Zhu, "Compact UWB bandpass filter using stub-loaded multiple-mode resonator," *IEEE Microwave and Wireless Components Letters*, Vol. 17, No. 1, 40–42, Jan. 2007.

[22] Ishii, H., T. Kimura, N. Kobayashi, A. Saito, Z. Ma, and S. Ohshima, "Development of UWB HTS bandpass filters with microstrip stubs-loaded three-mode resonator," *IEEE Transactions on Applied Superconductivity*, Vol. 23, No. 3, 1 500 204–1 500 204, Jun. 2013.

[23] Feng, W., X. Gao, W. Che, W. Yang, and Q. Xue, "LTCC wideband bandpass filters with high performance using coupled lines with open/shorted stubs," *IEEE Transactions on Components, Packaging and Manufacturing Technology*, Vol. 7, No. 4, 602–609, Apr. 2017.

[24] Feng, W., X. Gao, W. Che, and Q. Xue, "Bandpass filter loaded with open stubs using dual-mode ring resonator," *IEEE Microwave and Wireless Components Letters*, Vol. 25, No. 5, 295–297, May 2015.